Chinese Chemical Letters 33 (2022) 3993–3998

Contents lists available at ScienceDirect

Chinese Chemical Letters

journal homepage: www.elsevier.com/locate/cclet

# Uncovering growth species of multivariate MOFs in liquid phase by mass spectrometry

Jinli Han[a,b], Suming Chen[c], Xiaochun Zhou[b,*], Hexiang Deng[a,c,*]

[a] Key Laboratory of Biomedical Polymers-Ministry of Education, College of Chemistry and Molecular Sciences, Wuhan University, Wuhan 430072, China
[b] Division of Advanced Nanomaterials, Suzhou Institute of Nano-tech and Nano-bionics, Chinese Academy of Sciences, Suzhou 215125, China
[c] The Institute for Advanced Studies, Wuhan University, Wuhan 430072, China

ARTICLE INFO

*Article history:*
Received 16 October 2021
Revised 9 November 2021
Accepted 10 November 2021
Available online 18 November 2021

*Keywords:*
Metal-organic framework
Multivariate MOFs
Mass spectrometry
Growth species
Self-assembly

ABSTRACT

The unveiling of MOF growth mechanism is hampered by the lack of fundamental knowledge about the very early stage of nucleation, especially the form and ratio of molecular species in the solution for crystal growth. Herein, we report the detection of growth species for a series of MOFs with mono-linker, Cu-MOF-2-BDC and Cu-MOF-2-NDC, and two linkers, MTV-MOF-2-$(C_4H_4)_x$, by high resolution ESI-MS, where a large variety of Cu-containing species are identified unambiguously. The solvent molecules such as $H_2O$, methanol and DMF participate in the formation of these species, other than ethanol. Furthermore, in the growth solution of MTV-MOF-2-$(C_4H_4)_x$, growth species containing two different organic linkers are observed. The feeding ratio is not the only factor controlling the distribution of growth species for MTV-MOFs, but also the solvent involves in coordination, an aspect usually overlooked previously.



Metal-organic framework (MOF) is a fast developing class of porous crystals constructed by linking organic linkers and metal containing joints by strong coordination bonds. These frameworks offer molecularly defined pore spaces within which matter can be manipulated and controlled with the implications on their gas storage and separation, chemical sensing and energy applications [1–6]. Multivariate MOF (MTV-MOF), is constructed by mixing organic linkers of identical size and coordination but carrying different functional groups. These functional groups exist in the same MOF single crystal without altering the framework topology, therefore the properties of MTV-MOFs are much more tuneable than the mono-linker counterparts [7], giving opportunities to create new pore environments for potential applications in catalytic and biological properties [8–10]. However, the spatial arrangements of multiple types of functional groups or metal clusters in bulk crystals are complicated, which is reflected in the discrepancy between feeding ratio and experimental ratio for the synthesis [11]. The spatial arrangements of organic linkers and metals are gradually unveiled by solid-state nuclear magnetic resonance (NMR) spectroscopy [12], X-ray photoelectron spectroscopy and atom probe tomography [13,14], however, it remains unclear that how these different organic linkers assemble in the solution and form molecular species at early nucleation stage in MTV-MOF growth solution.

Recently, both *ex situ* and *in situ* techniques have been developed to investigate MOF crystallization mechanisms, with the attempt to offer details to understand MOF formation, morphology evolution, and structure transition [15]. Electron microscopy [16–18], X-ray diffraction [19,20], and atomic force microscopy were also applied for the study of crystal nucleation and growth (Scheme 1) [21,22]. However, these techniques did not distinguish the molecular species in the growth solution, especially for bulk crystal of MTV-MOFs (Scheme 1). Qualitative analysis of these chemicals in growth solution has the potential to offer valuable information about basic structural units, which is favorable for understanding the initial coordination process of metal ions and organic linkers. Thanks to the developments of electrospray ionization mass spectrometry (ESI-MS), the information of molecular species in solution was obtained clearly for MOFs with mono-linker [23–27]. Here, this technique is demonstrated to effectively distinguish the different type of growth species with their characteristic molecular weights in the growth solution of MTV-MOFs (Scheme 1).

In this study, we report the use of high resolution ESI-MS for identification of metal-containing molecular species of different types for MOFs with mono-linker, Cu-MOF-2-BDC, Cu-MOF-2-NDC and Cu-MOF-2-BDC-$Cl_2$, and two linkers, MTV-MOF-2-$(C_4H_4)_x$ ($x$ is varied between 0 and 1), where multiple different types of metal-

* Corresponding authors.
*E-mail addresses:* xczhou2013@sinano.ac.cn (X. Zhou), hdeng@whu.edu.cn (H. Deng).

https://doi.org/10.1016/j.cclet.2021.11.035
1001-8417/

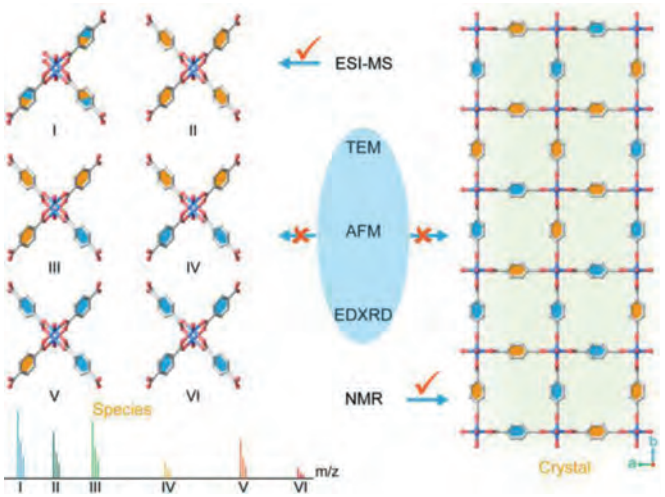


**Scheme 1.** Experimental approaches to study MTV-MOFs. Shown is the advantage of ESI-MS technique to uncover the types of growth species existing in MTV-MOF growth solution.

containing molecular species were assigned accurately in their growth solutions, including CuL (L: organic linker), $CuL_2$, $Cu_2L$, $Cu_2L_2$ and so on. Growth species of the same type but with different molecular weight were also observed, due to the coordination of various solvent molecules. Moreover, the molecular species were detected in MTV-MOF growth solution, and two different organic linkers could coordinate with the same metal ion to give different $Cu_x(LinkerA)_y(LinkerB)_z$-type molecular species. In addition, the discrepancy between feeding ratio and experimental ratio of different organic linkers is found to be related to the contents of different growth species of the same type, which is influenced by the solvents and coordination ability of organic linkers during the synthesis.

Specifically, we use a series of two dimensional (2D) porous MOFs with isoretucular structure (the same topology), Cu-MOF-2, to illustrate the ESI-MS method. The structure and property of MOFs were characterized prior to the ESI-MS analysis. Cu-MOF-2-BDC [28], constructed from paddle-while secondary building units (SBUs) and benzene-1,4-dicarboxylate (BDC) ligands to form a simple framework (Fig. S1 in Supporting information), is known to have isoreticular structures of various organic linker types, *e.g.*, naphthalene-1,4-dicarboxylic acid (NDC) for Cu-MOF-2-NDC and 2,5-dichloroterephthalic acid (BDC-$Cl_2$) for Cu-MOF-2-BDC-$Cl_2$ [29,30]. Cu-MOF-2-BDC crystals were synthesized using the similar procedure as reported with modifications for improving crystal crystallization rate. Mixed solvents (methanol, ethanol and *N*,*N*-dimethylformamide (DMF) with volumetric ratio of 1:1:4) were used rather than only pure DMF. The morphology of the Cu-MOF-2-BDC crystals was revealed by scanning electron microscopy (SEM), which showed a regular square shaped plate (Fig. S2 in Supporting information). The powder X-ray diffraction (PXRD) patterns of the as-synthesized crystals had a slightly shift comparing with the pattern simulated from single crystal structure data, due to the effects of the coordination molecules, where the solvents in our system were different from only pure DMF as solvent in previous study (Fig. S5 in Supporting information) [28]. Similar results were also observed in Cu-MOF-2-NDC system, where the regular square plated-shaped crystals were exhibited in SEM image (Fig. S3 in Supporting information), and PXRD patterns were in good agreement with simulated pattern demonstrating that this MOF possessed the well-defined 2D network structure, same like Cu-MOF-2-BDC (Fig. S6 in Supporting information). It was worth noting that the PXRD patterns of activated Cu-MOF-2-BDC and Cu-MOF-2-NDC also matched well, due to their identical topology (Figs. S1 and S7 in Supporting information). But their PXRD patterns differed from the corresponding as-synthesized samples, consistent with previous studies [28]. The structural transformation can be attributed the removal of solvent molecule from MOF crystal structure, which is common in MOF studies. The calculated Brunauer-Emmett-Teller (BET) surface areas of Cu-MOF-2-BDC and Cu-MOF-2-NDC were 150 and 12 $m^2/g$, respectively. The higher permanent porosity of the guest-free MOFs was observed in Cu-MOF-2-BDC due to the smaller steric hindrance of BDC in comparison to NDC (Figs. S1 and S8 in Supporting information).

In order to study the relationship between crystal structure and molecular species in MOF crystal formation process, it is critical to provide standard samples for comparison. First of all, the growth solution of pure Cu-MOF-2-BDC was detected by high-resolution ESI-MS, where a large variety of Cu-containing species were identified unambiguously. The mother liquor for MOF synthesis was filtered with nylon filters before injecting into the high-resolution ESI-MS. Multiple new peaks were identified in either the positive- or negative-ion spectra of mother liquor, other than in reference solutions (solvent, metal ions and organic linkers solutions), demonstrating the self-assembling of multiple Cu-containing molecular species in MOF growth solution (Figs. S11 and S13 in Supporting information). Accurate assignments of these growth species reveal their detailed chemical formulas with the reference to the theoretical isotopic distributions (Fig. 1, Fig. S12, Tables S2 and S3 in Supporting information). The relatively more abundant CuBDC-containing molecular species in Cu-MOF-2-BDC mother liquor were $[Cu(C_8H_5O_4)(HCON(CH_3)_2)_2]^+$, $[Cu(C_8H_5O_4)(HCON(CH_3)_2)]^+$, and $[Cu(C_8H_5O_4)(H_2O)(HCON(CH_3)_2)]^+$ in the positive-ion spectra, as well as $[Cu(C_8H_5O_4)(NO_3)_2]^-$ and $[Cu(C_8H_5O_4)_2(NO_3)]^-$ in the negative-ion spectra, respectively. The most abundant of these molecular species were $[Cu(C_8H_5O_4)(HCON(CH_3)_2)_2]^+$ and $[Cu(C_8H_5O_4)(NO_3)_2]^-$, in the positive-ion and negative-ion spectra, respectively. Surprisingly, the organic linker BDC containing two -COOH functional groups was only deprotonated on the side where the $Cu^{2+}$ was coordinated, while the exposed -COOH on the other side was not deprotonated, giving a CuL type species, for instance $[Cu(C_8H_5O_4)(NO_3)_2]^-$ in negative ion spectra (Fig. 1A, I). If the -COOH on both sides of BDC were deprotonated, these two -COOH would have been coordinated both with $Cu^{2+}$ at once to form $Cu_2L$ type species, such as $[Cu_2(C_8H_4O_4)(NO_3)_3]^-$ (Fig. 1A, III). Similarly, the Cu coordination sites in CuL type species could also capture one organic linker to form $CuL_2$ type species (Fig. 1A, II). Furthermore, $Cu_2L_2$ type species, *e.g.*, $[Cu_2(C_8H_4O_4)(C_8H_5O_4)(NO_3)_2]^-$ could be formed from $CuL_2$ species through removing one proton H and combing with $Cu^{2+}$ (Fig. 1A, VI). However, the low relative abundance of SBUs ($Cu_2L_4$, X in Fig. 1A) implies they are unlikely to be the direct growth units for the growth of MOFs.

Moreover, small solvent molecules such as DMF, methanol, $H_2O$ and anion $NO_3^-$ also coordinated with metal-containing species to give multiple growth species of same type, but with different molecular weight, $[Cu_2(C_8H_4O_4)(NO_3)_3]^-$ and $[Cu_2(C_8H_4O_4)(CH_3OH)(NO_3)_3]^-$ (Fig. 1A, III and IV) for instance. However, another common solvent molecule, ethanol, didn't participate in the formation of these species, indicating its weaker coordination to the metal ions. This provides valuable guidance to the choice of solvents for the synthesis of MOF crystals and their activation.

In addition to Cu-MOF-2-BDC, the metal-containing molecular species of other isoreticular MOF, Cu-MOF-2-NDC, were also evaluated, where the types of molecular species were similar to those for Cu-MOF-2-BDC. It is worth mentioning that the exact masses of BDC and NDC are respectively 166.0266 and 216.0423, and the exact mass of NDC is 50.0157 greater than that of BDC. Thus, it

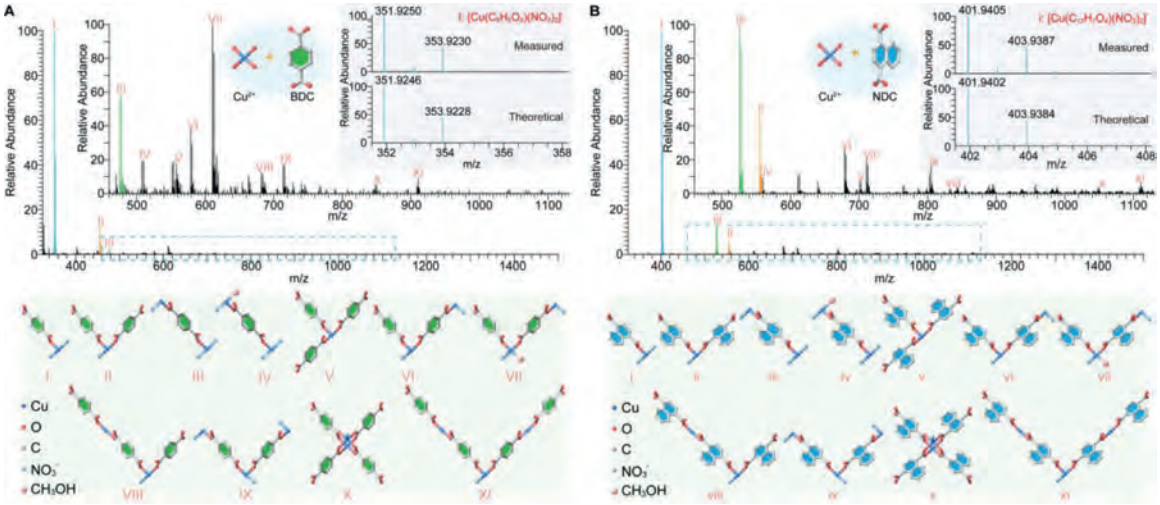


**Fig. 1.** High resolution ESI-MS spectra and assignments of different molecular species in Cu-MOF-2-BDC and Cu-MOF-2-NDC growth solutions. (A) Negative-ion spectrum of Cu-MOF-2-BDC obtained with full range of species and schematic diagrams of a series of Cu-containing molecular species ($Cu^{2+}$:BDC = 1:1, magnified image for blue dashed box from $m/z$ 460–1130 for optimum display of speciation). The inset provides confirmation of the chemical composition for the $[Cu(C_8H_5O_4)(NO_3)_2]^-$ species centered at $m/z$ ~352 through comparison of the measured and theoretical isotopic distributions. (B) Negative-ion spectrum of Cu-MOF-2-NDC obtained with full range of species and schematic diagrams of a series of Cu-containing molecular species ($Cu^{2+}$:NDC = 1:1, magnified image for blue dashed box from $m/z$ 460–1130 for optimum display of speciation). The inset provides confirmation of the chemical composition for the $[Cu(C_{12}H_7O_4)(NO_3)_2]^-$ species centered at $m/z$ ~402 through comparison of the measured and theoretical isotopic distributions.

is facile to assign these same types of molecular species of Cu-MOF-2-NDC from ESI-MS spectra based on the results of Cu-MOF-2-BDC. Specifically, the exact masses of CuL-type and $CuL_2$-type species in Cu-MOF-2-NDC growth solution ought to be 50.0157 and 100.0314 greater than those of Cu-MOF-2-BDC, respectively (Tables S2 and S3). Indeed, all types of molecular species in Cu-MOF-2-BDC growth solution were also detected in Cu-MOF-2-NDC mother liquor unambiguously (Table S3). Similarly, the most abundant of these species were $[Cu(C_{12}H_7O_4)(HCON(CH_3)_2)_2]^+$ and $[Cu(C_{12}H_7O_4)(NO_3)_2]^-$, in the positive-ion and negative-ion spectra, respectively, and the measured isotopic distributions of each species matched well with the theoretical spectra, confirming the accuracy of molecular species assignments (Fig. 1B).

Furthermore, this finding that the molecular species in the growth solution of these two isoreticular MOFs were similar to each other provides the chemical bases for the construction of MTV-MOFs with functionality variance [7]. MTV-MOF-2-$(C_4H_4)_x$ was chosen here for the study of growth species and the exploration of their the self-assembly from metal ions and linkers. Prior to study it, the characterizations of this MTV-MOF were carried out. In MTV-MOF-2-$(C_4H_4)_x$, although the different functional groups (-H in BDC, -$C_4H_4$ in NDC) appended to the same backbones, the framework topology did not change based on their PXRD patterns (Fig. S7). The crystals were synthesized using the similar experimental procedures of Cu-MOF-2-BDC and the feeding ratio of BDC to NDC was 1 (Section 1 in Supporting information). The MTV-MOF-2-$(C_4H_4)_x$ was a regular square shaped plate, similar to that of Cu-MOF-2-NDC (Figs. S3 and S4 in Supporting information). The calculated BET surface area of MTV-MOF-2-$(C_4H_4)_x$ was 94 $m^2/g$, in between those of Cu-MOF-2-BDC and Cu-MOF-2-NDC (Fig. S8 in Supporting information). The exact ratio of organic linkers, BDC to NDC, in MTV-MOF-2-$(C_4H_4)_x$ crystals was further obtained from the $^1H$ NMR spectroscopy of an HCl-digested solution of bulk samples, which was in a good agreement with elemental analysis results (Figs. S9, S10 and Table S1 in Supporting information). Nevertheless, a critical remain unanswered is why these different organic linkers can be self-assembly into the same MOF backbone without changing the framework topology.

In the attempt to answer this challenging question, the mother liquor of MTV-MOF-2-$(C_4H_4)_x$ was also detected by high resolution ESI-MS, where the molecular species in the growth solution were assigned precisely to give accurate chemical formulae (Fig. 2). In addition to the same Cu-containing species observed in the study of pure Cu-MOF-2, new molecular species containing two different organic linkers were observed. Typically, most of molecular species of Cu-MOF-2-BDC and Cu-MOF-2-NDC were observed in growth solution of MTV-MOF-2-$(C_4H_4)_x$ except some CuBDC-containing growth species, indicating that the coordination mode of the metal ion and the organic linkers remained unchanged under the same synthetic condition (Figs. 2A and C). But the strength of coordination formed using different organic linkers was different. The more abundant CuL-containing molecular species in growth solutions were $[Cu(C_{12}H_7O_4)(HCON(CH_3)_2)_2]^+$ and $[Cu(C_8H_5O_4)(HCON(CH_3)_2)_2]^+$ in the positive-ion spectra, as well as $[Cu(C_{12}H_7O_4)(NO_3)_2]^-$ and $[Cu(C_8H_5O_4)(NO_3)_2]^-$ in the negative-ion spectra, while the most abundant species were $[Cu(C_{12}H_7O_4)(HCON(CH_3)_2)_2]^+$ and $[Cu(C_{12}H_7O_4)(NO_3)_2]^-$, in the positive-ion and negative-ion spectra of MTV-MOF-2-$(C_4H_4)_x$, respectively. The results showed that the relative content of CuNDC-containing molecular species in growth solution was higher than that of CuBDC-containing molecular species when the feeding ratio of BDC to NDC was 1, without considering the difference in ionization efficiency of similar growth species. This indicated that the strength of coordination formed by NDC is greater than that of BDC. This is in good accordance to the experimental ratio of BDC and NDC in bulk crystal obtained from the $^1H$ NMR spectroscopy, where the experimental ratio of BDC to NDC was less than 1 with equal amount of linkers in starting materials (Fig. 3A and Fig. S10). Moreover, two different organic linkers, BDC and NDC can coordinate with the same $Cu^{2+}$ to give the $Cu_xL_{BDC}L_{NDC}$-type species, which were detected in positive and negative-ion spectra of MTV-MOF-2-$(C_4H_4)_x$ (II, VI, VII, VIII, IX, X and XI in Fig. 2C). Therefore, $CuL_2$-type species possessed three forms with different molecular weight, including $Cu(L_{BDC})_2$, $Cu(L_{NDC})_2$ and $Cu(L_{BDC})(L_{NDC})$, and the relative content of these molecular species varied with the feeding ratio of BDC to NDC (Figs. 2B and 3B). Based on the results of $CuL_2$-type species, similarly, the $Cu_2L_3$-type species should include four different forms, if BDC and NDC coordinated with the same $Cu^{2+}$. Indeed, $Cu_2(L_{BDC})_2(L_{NDC})$, $Cu_2(L_{BDC})(L_{NDC})_2$ and $Cu_2(L_{NDC})_3$ were detected except $Cu_2(L_{BDC})_3$ in growth solution of MTV-MOF-

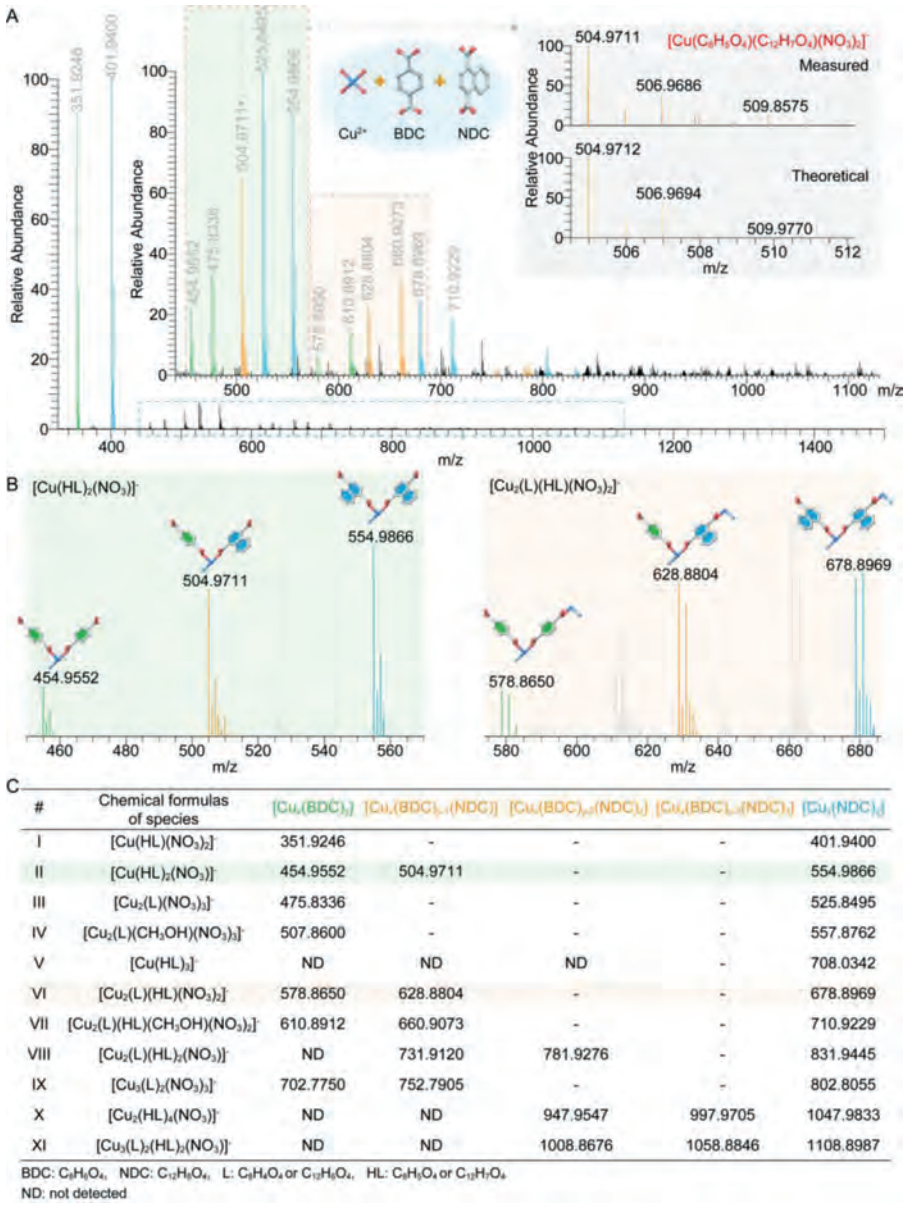


C

| # | Chemical formulas of species | $[Cu_x(BDC)_y]$ | $[Cu_x(BDC)_{y-1}(NDC)]$ | $[Cu_x(BDC)_{y-2}(NDC)_2]$ | $[Cu_x(BDC)_{y-3}(NDC)_3]$ | $[Cu_x(NDC)_y]$ |
|---|---|---|---|---|---|---|
| I | $[Cu(HL)(NO_3)_2]^-$ | 351.9246 | - | - | - | 401.9400 |
| II | $[Cu(HL)_2(NO_3)]^-$ | 454.9552 | 504.9711 | - | - | 554.9866 |
| III | $[Cu_2(L)(NO_3)_3]^-$ | 475.8336 | - | - | - | 525.8495 |
| IV | $[Cu_2(L)(CH_3OH)(NO_3)_3]^-$ | 507.8600 | - | - | - | 557.8762 |
| V | $[Cu(HL)_2]^-$ | ND | ND | ND | - | 708.0342 |
| VI | $[Cu_2(L)(HL)(NO_3)_2]^-$ | 578.8650 | 628.8804 | - | - | 678.8969 |
| VII | $[Cu_2(L)(HL)(CH_3OH)(NO_3)_2]^-$ | 610.8912 | 660.9073 | - | - | 710.9229 |
| VIII | $[Cu_2(L)(HL)_2(NO_3)]^-$ | ND | 731.9120 | 781.9276 | - | 831.9445 |
| IX | $[Cu_3(L)_2(NO_3)_3]^-$ | 702.7750 | 752.7905 | - | - | 802.8055 |
| X | $[Cu_2(HL)_4(NO_3)]^-$ | ND | ND | 947.9547 | 997.9705 | 1047.9833 |
| XI | $[Cu_3(L)_2(HL)_2(NO_3)]^-$ | ND | ND | 1008.8676 | 1058.8846 | 1108.8987 |

BDC: $C_8H_6O_4$, NDC: $C_{12}H_8O_4$, L: $C_8H_4O_4$ or $C_{12}H_6O_4$, HL: $C_8H_5O_4$ or $C_{12}H_7O_4$
ND: not detected

**Fig. 2.** High resolution ESI-MS spectra and assignments of molecular species in MTV-MOF-2-$(C_4H_4)_x$ growth solutions. (A) Negative-ion spectrum of MTV-MOF-2-$(C_4H_4)_x$ obtained with full range of species ($Cu^{2+}$:organic linkers = 1:1 and BDC:NDC = 1:1, magnified image for blue dashed box from $m/z$ 440–1130 for optimum display of speciation). The inset provides confirmation of the chemical composition for the $[Cu(C_8H_5O_4)(C_{12}H_7O_4)(NO_3)]^-$ species centered at $m/z$ ~505 through comparison of the measured and theoretical isotopic distributions. (B) Negative-ion spectra of $CuL_2$-type and $Cu_2L_2$-type species. (C) The detailed assignments of all growth species in negative-ion spectra of MTV-MOF-2-$(C_4H_4)_x$. Green and orange backgrounds in (C) correspond to the species in (B).

2-$(C_4H_4)_x$. The absence of $Cu_2(L_{BDC})_3$ is likely attributed to the weak coordination for BDC, further confirming the stronger coordination of NDC with $Cu^{2+}$ in comparison to that of BDC (Fig. 2C, VIII).

In order to further study the impact from different feeding ratio of organic linkers for these different $CuL_2$-type species, high resolution ESI-MS spectra were also obtained for MTV-MOF-2-$(C_4H_4)_x$ with different feeding ratios of BDC to NDC (Figs. S15 and S17 in Supporting information). There was no obvious change in the types of growth species, however, the relative content of these growth species varied drastically (Figs. 3B-D and Figs. S15-S17 in Supporting information). In order to compare the changing trends of growth species under different conditions, $CuL_2$-type species was chosen here to illustrate the influence of different feeding ratios, where the relative abundance of the most abundant of molecular species in each spectrum was defined as 100% (Fig. 3B). Specifically, when the feeding ratio of BDC to NDC was 3:1, the fraction of $Cu(L_{BDC})_2$ species present the most within $CuL_2$-type species, while that of $Cu(L_{NDC})_2$ species was the least, indicating that the probability of $Cu^{2+}$ coordinating with BDC was greater than that with NDC, when BDC is more abundant in the solution (Fig. 3B). These results were in stark contrast to those of the feeding ratio of BDC to NDC was 1:3, where the fractions of $Cu(L_{BDC})_2$ and $Cu(L_{NDC})_2$ species were respectively the least and most within $CuL_2$-type species. It was not surprising that NDC-containing molecular species were major species in the case of excess NDC. However, when the feeding ratio of BDC to NDC was 1, the fraction of $Cu(L_{NDC})_2$ species was also much greater than that of $Cu(L_{BDC})_2$ species, demonstrated that $Cu^{2+}$ tended to coordinate with NDC rather than BDC in growth solution. Moreover,

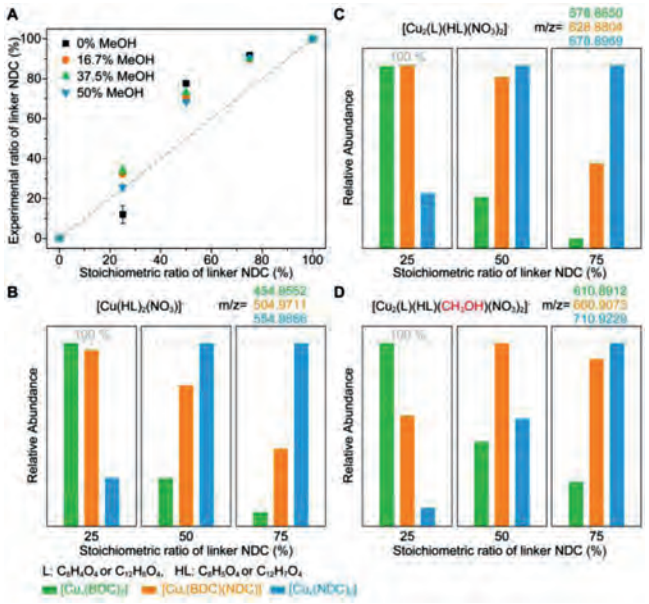


**Fig. 3.** The change trends of NDC actual ratio in its bulk crystals and relative contents of different $CuL_2$-type and $Cu_2L_2$-type species in MTV-MOF-2-$(C_4H_4)_x$ growth solution. (A) The change trends of NDC actual ratio with different feeding ratio in MTV-MOF-2-$(C_4H_4)_x$ bulk crystals. (B-D) Relative contents of $CuL_2$-type and $Cu_2L_2$-type species in growth solution at different feeding ratios of BDC to NDC.

other molecular species such as $Cu_2L_2$-type species also fellow above rules, further confirming the coordination of NDC with $Cu^{2+}$ is stronger than that of BDC. This finding was also revealed from the positive-ion spectra, where the fraction of $Cu_2(L_{BDC})_2$ species decreased with the ratio of NDC increasing (Fig. S16). This demonstrated that BDC in $Cu(L_{BDC})_2$ and $Cu(L_{BDC})(L_{NDC})$ species prefers to be replaced by NDC to respectively form $Cu(L_{BDC})(L_{NDC})$ and $Cu(L_{NDC})_2$ species in the case of abundant NDC, confirming the difference in coordination ability of similar organic linkers. More interestingly, the small solvent also plays a critical role during the assembling process, while the addition of methanol favors to the formation of CuNDC containing species at low NDC to BDC ratio, but this role is not obvious at high NDC to BDC ratio (Fig. 3A). This shows that solvent molecule participate in the MOF formation process, and will change the content of linkers in the resulting MTV-MOFs. In short, the solvent is considered as a critical factor to control the ratio of linkers in MTV-MOFs, which was usually ignored in the early conducted research studies.

Furthermore, the initial growth solution of MTV-MOF-2-$(C_4H_4)_x$ was also assessed by ESI-MS at room temperature, where the types of molecular species in growth solution were similar to those of sample synthesized 1 h at 70 °C, but the relative abundance of molecular species in these two experiments was different, confirming that the temperature and reaction time has an effect on self-assembly of species. The solution was prepared by mixing metal ions and organic linkers directly at room temperature, the similar negative-ion spectrum demonstrated that the formation these molecular species would be formed once the metal ions contacted with the organic linkers, which is a fast process (Fig. S17).

In addition, the ESI-MS was further successfully applicable to probe another isoreticular MOF, *e.g.*, Cu-MOF-2-BDC-$Cl_2$, where the types of molecular species in growth solution were similar to those of other two isoreticular MOFs. The MOF growth solution was prepared *via* a similar condition of Cu-MOF-2-BDC (Section 1 in Supporting information). Specifically, the exact mass of BDC-$Cl_2$ is 233.9487 and 67.9221 greater than that of BDC, thus these same types of growth species in spectra of isoreticular Cu-MOF-2-BDC-$Cl_2$ could be assign facilely. Indeed, multiple types of molecular species in Cu-MOF-2-BDC growth solution were also detected in Cu-MOF-2-BDC-$Cl_2$ growth solution with organic linkers BDC were replaced by BDC-$Cl_2$ and the most abundant of these species were $[Cu(C_8H_3Cl_2O_4)(HCON(CH_3)_2)_2]^+$ and $[Cu(C_8H_3Cl_2O_4)(NO_3)_2]^-$, in the positive-ion and negative-ion spectra, respectively (Figs. S18 and S19 in Supporting information). The similar results of molecular species detected by high resolution ESI-MS demonstrated the universality of this useful technique for tracking molecular species in MOF growth solution.

In summary, a large variety of metal-containing growth species of a series of MOFs with mono-linker and two linkers were identified unambiguously by high resolution ESI-MS. Small solvent molecules such as $H_2O$, methanol and DMF participated in the coordination of growing species. The relative content of different organic linkers in bulk MTV-MOF crystals, originated from content of organic linkers in various molecular species in the growth solution, was influenced by the feeding ratio and the strength of coordination bond form by different linkers. One important observation is that the solvent molecules participate in the MOF formation process, and will change the content of linkers in the resulting MTV-MOFs. These findings, based on exploration in coordination molecules of metal ions and organic linkers by high resolution ESI-MS, provide new insight to understand the formation of isoreticular MOFs and MTV-MOFs.

## Declaration of competing interest

The authors declare that they have no known competing financial interests or personal relationships that could have appeared to influence the work reported in this paper.

## Acknowledgments

We thank W. Wang, S. Li and J. Liu for their valuable advice on this research. We also thank the Core Research Facilities of College of Chemistry and Molecular Sciences at Wuhan University for assistance on material characterizations, The State Key Laboratory of Coordination Chemistry (SKLCC) at Nanjing University for high resolution ESI-MS characterizations. We acknowledge support from the National Natural Science Foundation of China (Nos. 91545205, 91622103, 21971199 and 22025106), National Key Research and Development Project (Nos. 2020YFB1505700, 2016YFA0200700 and 2018YFA-0704000), Innovation Team of Wuhan University (No. 2042017kf0232) and the Fundamental Research Funds for the Central Universities (No. 2042020kf0214).

## Supplementary materials

Supplementary material associated with this article can be found, in the online version, at doi:10.1016/j.cclet.2021.11.035.

## References

[1] O.M. Yaghi, M. O'Keeffe, N.W. Ockwig, et al., Nature 423 (2003) 705–714.
[2] S. Kitagawa, R. Kitaura, S.I. Noro, Angew. Chem. Int. Ed. 43 (2004) 2334–2375.
[3] H. Furukawa, K.E. Cordova, M. O'Keeffe, O.M. Yaghi, Science 341 (2013) 1230444.
[4] H.S. Cho, H. Deng, K. Miyasaka, et al., Nature 527 (2015) 503–507.
[5] H. Zeng, M. Xie, T. Wang, et al., Nature 595 (2021) 542–548.
[6] Z. Hu, B.J. Deibert, J. Li, Chem. Soc. Rev. 43 (2014) 5815–5840.
[7] H. Deng, C.J. Doonan, H. Furukawa, et al., Science 327 (2010) 846–850.
[8] K.M. Choi, K. Na, G.A. Somorjai, O.M. Yaghi, J. Am. Chem. Soc. 137 (2015) 7810–7816.
[9] Z. Dong, Y. Sun, J. Chu, X. Zhang, H. Deng, J. Am. Chem. Soc. 139 (2017) 14209–14216.
[10] M. Kalaj, J.M. Palomba, K.C. Bentz, S.M. Cohen, Chem. Commun. 55 (2019) 5367–5370.
[11] W. Xu, B. Tu, Q. Liu, et al., Nat. Rev. Mater. 5 (2020) 764–779.

[12] X. Kong, H. Deng, F. Yan, et al., Science 341 (2013) 882–885.
[13] Q. Liu, H. Cong, H. Deng, J. Am. Chem. Soc. 138 (2016) 13822–13825.
[14] Z. Ji, T. Li, O.M. Yaghi, Science 369 (2020) 674–680.
[15] M.J. Van Vleet, T. Weng, X. Li, J.R. Schmidt, Chem. Rev. 118 (2018) 3681–3721.
[16] J. Xing, L. Schweighauser, S. Okada, K. Harano, E. Nakamura, Nat. Commun. 10 (2019) 3608.
[17] J.P. Patterson, P. Abellan, M.S. Denny, et al., J. Am. Chem. Soc. 137 (2015) 7322–7328.
[18] X. Liu, S.W. Chee, S. Raj, et al., Proc. Natl. Acad. Sci. U. S. A. 118 (2021) e2008880118.
[19] J. Cravillon, C.A. Schröder, R. Nayuk, et al., Angew. Chem. In. Ed. 50 (2011) 8067–8071.
[20] F. Millange, M.I. Medina, N. Guillou, et al., Angew. Chem. Int. Ed. 49 (2010) 763–766.
[21] M. Shoaee, M.W. Anderson, M.P. Attfield, Angew. Chem. Int. Ed. 47 (2008) 8525–8528.
[22] N. Hosono, A. Terashima, S. Kusaka, R. Matsuda, S. Kitagawa, Nat. Chem. 11 (2019) 109–116.
[23] J.A. Rood, W.C. Boggess, B.C. Noll, K.W. Henderson, J. Am. Chem. Soc. 129 (2007) 13675–13682.
[24] G. Seeber, G.J.T. Cooper, G.N. Newton, et al., Chem. Sci. 1 (2010) 62–67.
[25] I.H. Lim, W. Schrader, F. Schüth, Chem. Mater. 27 (2015) 3088–3095.
[26] R. Wagia, I. Strashnov, M.W. Anderson, M.P. Attfield, Angew. Chem. Int. Ed. 55 (2016) 9075–9079.
[27] M.H. Rosnes, F.S. Nesse, M. Opitz, P.D.C. Dietzel, Microporous Mesoporous Mater. 275 (2019) 207–213.
[28] C.G. Carson, K. Hardcastle, J. Schwartz, et al., Eur. J. Inorg. Chem. 2009 (2009) 2338–2343.
[29] P. Kanoo, K.L. Gurunatha, T.K. Maji, J. Mater. Chem. 20 (2010) 1322–1331.
[30] M. Eddaoudi, J. Kim, D. Vodak, et al., Proc. Natl. Acad. Sci. U. S. A. 99 (2002) 4900–4904.